

# Chiral three-nucleon forces for the new local position-space two-nucleon potential in *ab initio* many-body calculations

R. Z. Hu <sup>1</sup> J. G. Li <sup>2,3</sup> S. Q. Fan <sup>1</sup> and F. R. Xu <sup>1,2,3,\*</sup>

<sup>1</sup>*School of Physics, and State Key Laboratory of Nuclear Physics and Technology, Peking University, Beijing 100871, China*

<sup>2</sup>*Institute of Modern Physics, Chinese Academy of Sciences, Lanzhou 730000, China*

<sup>3</sup>*Southern Center for Nuclear-Science Theory (SCNT),*

*Institute of Modern Physics, Chinese Academy of Sciences, Huizhou 516000, China*

(Dated: June 23, 2026)

Three-nucleon force (3NF) plays an important role in understanding the structure of finite nuclei and the saturation properties of infinite nuclear matter. More specifically, 3NF should be necessary for each two-nucleon force (2NF) to obtain more accurate description of nuclear systems. 3NF derived from the chiral effective field theory has been successful in *ab initio* calculations of atomic nuclei. Most of established chiral nuclear forces have a nonlocal form in the momentum space. In this work, we construct a companion chiral 3NF specifically tailored to the new Idaho local position-space 2NF, and calculate binding energies and radii of nuclei up to  $^{132}\text{Sn}$ . We find that a chiral 3NF with hybrid local and nonlocal regulators has advantages in improving the nuclear structure calculations of both binding energies and radii with the new Idaho 2NF. The two low-energy constants of 3NF are constrained by the ground-state energies of  $^3\text{H}$  and  $^{16}\text{O}$  as suggested in a recent work.

## I. INTRODUCTION

One of the main goals of *ab initio* nuclear theory is to understand atomic nuclei and nuclear matter from the fundamental degrees of freedom and interactions [1, 2]. Within the framework of the chiral effective field theory ( $\chi\text{EFT}$ ), two-nucleon and three-nucleon forces (2NF and 3NF, respectively) naturally emerge at different orders arranged by a proper power counting scheme [3, 4]. At a given chiral order, chiral nucleon interactions are renormalized by multiplying regulator functions that suppress high-momentum contributions beyond a certain cutoff momentum [5, 6]. Low-energy constants (LECs) appearing in chiral interactions are determined by available experimental data [7–9]. Chiral Hamiltonians obtained thus have been successfully applied to *ab initio* calculations of strongly correlated many-body nuclei and nuclear matter [10–23].

Nevertheless, open questions still remain for  $\chi\text{EFT}$ -based nuclear forces. One of the most important questions is whether the chiral interaction can simultaneously reproduce experimental ground-state energies and charge radii of medium-mass nuclei, and the saturation properties of nuclear matter [4, 21, 24–27]. Though many efforts have been made to address this issue by including many-body observables in the determination of 3NF LECs or by introducing different regularization schemes [28–39], the situation is still unclear, and further investigations are needed [40–52]. While previous studies indicate that hybrid local-nonlocal (lnl) 3NF regulators can improve the simultaneous description of nuclear energies and radii compared with purely local regulators, a systematic underestimation of charge radii persists [32].

Most of previous nuclear *ab initio* calculations were

based on nonlocal momentum-space potentials. Local position-space potentials were explored mainly for light-mass nuclei ( $A \lesssim 16$ ) using quantum Monte Carlo (QMC) methods [53–63]. However, the situation for heavier nuclei is barely known due to the computation limits of QMC methods. In this work, we construct a companion chiral 3NF specifically tailored to the new Idaho local position-space 2NF [64], and perform a systematic comparison between local and hybrid lnl 3NF regulators with the new family of 2NF plus 3NF. These should be useful for future *ab initio* nuclear structure calculations.

## II. CHIRAL THREE-NUCLEON FORCES AND REGULATORS

The  $A$ -body intrinsic Hamiltonian can be written as

$$\hat{H} = \frac{1}{A} \sum_{i < j}^A \frac{(\mathbf{p}_i - \mathbf{p}_j)^2}{2m} + \sum_{i < j}^A \hat{V}_{\text{NN}}^{ij} + \sum_{i < j < k}^A \hat{V}_{\text{3N}}^{ijk}, \quad (1)$$

where the first term denotes the intrinsic kinetic energy, whereas  $\hat{V}_{\text{NN}}$  and  $\hat{V}_{\text{3N}}$  indicate 2NF and 3NF, respectively. In the present work, to improve many-body calculations, we want to construct a chiral 3NF which complements the chiral local position-space 2NF developed recently by the Idaho group [64]. The local position-space 2NF was obtained by the chiral expansion up to the  $\text{N}^3\text{LO}$  with a position-space regulator cutoff  $R_\pi = 1.2$  fm [64]. To speed up the convergences of many-body calculations of medium-mass nuclei, the 2NF is evolved to a low-momentum scale  $\lambda = 2.2 \text{ fm}^{-1}$  using the similarity renormalization group (SRG) [65, 66]. The resulting low-resolution 2NF has been successfully applied to *ab initio* no-core shell model (NCSM) calculations of low-lying states and electromagnetic properties of  $^{10}\text{B}$  [67, 68]. We have checked that the  $\lambda$  dependence of the results can

\* Corresponding author: frxu@pku.edu.cn

be largely absorbed by adjusting the 3NF LECs, which equivalently considers induced-3NF effects.

The chiral 3NF at N<sup>2</sup>LO consists of three topologies [69, 70],

$$\hat{V}_{3N} = \hat{V}_{3N}^{2\pi} + \hat{V}_{3N}^{1\pi} + \hat{V}_{3N}^{\text{ct}}. \quad (2)$$

The long-range two- $\pi$  exchange term  $\hat{V}_{3N}^{2\pi}$  contains three pion-nucleon ( $\pi N$ ) scattering LECs which take  $c_1 = -0.74 \text{ GeV}^{-1}$ ,  $c_3 = -3.61 \text{ GeV}^{-1}$  and  $c_4 = 2.44 \text{ GeV}^{-1}$  [38, 64, 71] determined by the Roy-Steiner-equation scattering analysis at N<sup>2</sup>LO [71, 72]. The intermediate-range one-pion exchange  $\hat{V}_{3N}^{1\pi}$  and short-range three-nucleon contact term  $\hat{V}_{3N}^{\text{ct}}$  contain two additional LECs,  $c_D$  and  $c_E$ , respectively.

Similar to the 2NF, the chiral 3NF also needs to be applied with regulator functions to suppress high-momentum contributions. Several forms of the regulator function have been proposed, including the local form [73]

$$f_{\text{local}} = \exp \left[ - \left( \frac{|\mathbf{p}'_2 - \mathbf{p}_2|^2}{\Lambda^2} \right)^2 - \left( \frac{|\mathbf{p}'_3 - \mathbf{p}_3|^2}{\Lambda^2} \right)^2 \right], \quad (3)$$

the nonlocal form [70]

$$f_{\text{nonlocal}} = \exp \left[ - \left( \frac{4p^2 + 3q^2}{4\Lambda'^2} \right)^2 - \left( \frac{4p'^2 + 3q'^2}{4\Lambda'^2} \right)^2 \right], \quad (4)$$

and the hybrid local-nonlocal (lnl) form [32]

$$f_{\text{lnl}} = f_{\text{local}} f_{\text{nonlocal}}, \quad (5)$$

with  $\mathbf{p}_i$  ( $\mathbf{p}'_i$ ) being the initial (final) momentum of  $i$ th nucleon,  $p$  and  $q$  ( $p'$  and  $q'$ ) being the magnitude of initial (final) Jacobi momenta.  $\Lambda$  ( $\Lambda'$ ) is the  $\chi$ EFT hard cutoff. We have tested the two different regularization schemes to see the difference. The cutoffs are set to be  $\Lambda = 500 \text{ MeV}$  for the local regulator, and  $\Lambda = 700 \text{ MeV}$  and  $\Lambda' = 500 \text{ MeV}$  for the lnl regulator. Other different cutoffs of  $\Lambda$  ( $\Lambda'$ ) have also been tested, obtaining similar results without conclusions changed.

### III. PARAMETERIZATION OF LECs $c_D$ AND $c_E$ OF CHIRAL THREE-NUCLEON FORCE

There is still no unified agreement on strategies to constrain the 3NF LECs  $c_D$  and  $c_E$  [28, 35, 38, 73]. However, at least two uncorrelated observables are required to determine  $c_D$  and  $c_E$  values. In this work, we use the  ${}^3\text{H}$  ground-state energy  $E({}^3\text{H})$  as the first constraint on  $c_D$  and  $c_E$ . Though there have been attempts to use the binding energy or charge radius of  ${}^4\text{He}$  as the second constraint [74, 75], in many cases this strategy does not seem to be a good choice [35], primarily due to the strong correlation between these observables [76]. The  $\beta$ -decay half-life of  ${}^3\text{H}$  may be used as a constraint [76–82], because  $c_D$

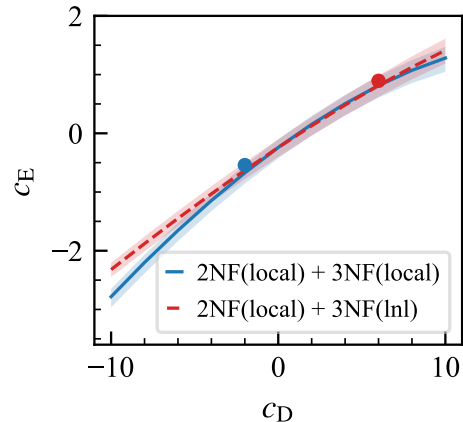


FIG. 1. Relation between  $c_D$  and  $c_E$  obtained by the constraint of the  ${}^3\text{H}$  binding energy, for the local and lnl 3NF regulators. Shadows indicate the EFT uncertainty of 300 keV. The blue and red filled dots are the final optimized results by considering the  ${}^{16}\text{O}$  binding energy for 2NF(local)+3NF(local) and 2NF(local)+3NF(lnl), respectively.

also appears in the short-range two-nucleon axial-vector current of the  $\beta$  decay. In the recent work [35], it was suggested to use the  ${}^{16}\text{O}$  ground-state energy  $E({}^{16}\text{O})$  as a constraint which we follow in the present work.

The  ${}^3\text{H}$  energy is calculated using the NCSM in the Jacobi coordinates [83]. The calculation is converged at a harmonic oscillator (HO) frequency around  $\hbar\Omega = 24 \text{ MeV}$  with  $N_{\text{max}} = 44$  HO shells. The  ${}^3\text{H}$  NCSM calculation with such large model space should be considered to be exact, and the many-body uncertainty should be ignored. The dominant uncertainty should be from the  $\chi$ EFT truncation. The new Idaho 2NF is truncated at the N<sup>3</sup>LO level [64]. Uncertainties caused by  $\chi$ EFT can be estimated, e.g., for an observable  $X$  at N<sup>2</sup>LO and N<sup>3</sup>LO, via [84–86]

$$\Delta X_{\text{N}^2\text{LO}} = \max \left( Q^4 |X_{\text{LO}}|, Q^2 |X_{\text{LO}} - X_{\text{NLO}}|, Q |X_{\text{NLO}} - X_{\text{N}^2\text{LO}}| \right), \quad (6)$$

and

$$\Delta X_{\text{N}^3\text{LO}} = \max \left( Q^5 |X_{\text{LO}}|, Q^3 |X_{\text{LO}} - X_{\text{NLO}}|, Q^2 |X_{\text{NLO}} - X_{\text{N}^2\text{LO}}|, Q |X_{\text{N}^2\text{LO}} - X_{\text{N}^3\text{LO}}| \right), \quad (7)$$

respectively, where  $Q$  is the EFT expansion scale measured by the ratio of the nucleon momentum transfer over the EFT hard cutoff  $\Lambda$ , which can be estimated by the pion mass over  $\Lambda$ . For  $\Lambda \approx 600 \text{ MeV}$ , the typical value is  $Q \approx 1/3$  [35, 76] which is used in quantifying the EFT uncertainty. We have estimated that uncertainties from the  $\chi$ EFT truncation at N<sup>2</sup>LO and N<sup>3</sup>LO are 446

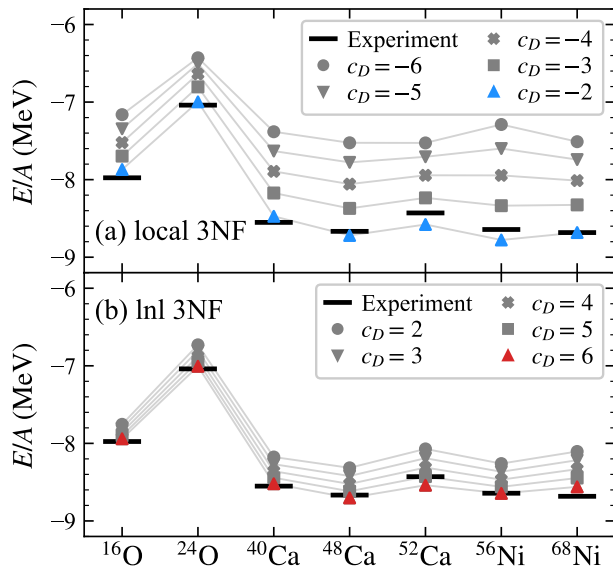


FIG. 2. Ground-state energies of selected medium-mass doubly-closed-shell nuclei, calculated by IMSRG with increasing the  $c_D$  value in a step of 1.0, starting from  $c_D = -6.0$  for the local 3NF regulator (a), and from  $c_D = 2.0$  for the lnI regulator (b). The black bars indicate experimental data [87].

keV and 149 keV, respectively, for the  ${}^3\text{H}$  ground-state energy. Therefore, in optimizing the 3NF LECs  $c_D$  and  $c_E$ , we do not use experimental data to strictly constrain the binding energy of  ${}^3\text{H}$ , whereas we allow the calculated energy to vary around the experimental value in a suitable range (approximately 300 keV) estimated with theoretical uncertainty. The constraint imposed by the  ${}^3\text{H}$  binding energy thus yields a correlation band between  $c_D$  and  $c_E$ , as illustrated in Fig. 1.

As suggested in Ref. [35], the  ${}^{16}\text{O}$  ground-state energy is used as another constraint to fix the values of  $c_D$  and  $c_E$ . We use the IMSRG in the Magnus formulation [88, 89] to calculate the  ${}^{16}\text{O}$  ground-state energy. The many-body Hamiltonian is normal ordered with respect to the reference state of the Hartree-Fock ground state as [90, 91]

$$\hat{H} = E_0 + \sum_{ij} f_{ij} \{\hat{a}_i^\dagger \hat{a}_j\} + \frac{1}{2!^2} \sum_{ijkl} \Gamma_{ijkl} \{\hat{a}_i^\dagger \hat{a}_j^\dagger \hat{a}_l \hat{a}_k\} + \frac{1}{3!^2} \sum_{ijklmn} W_{ijklmn} \{\hat{a}_i^\dagger \hat{a}_j^\dagger \hat{a}_k^\dagger \hat{a}_n \hat{a}_m \hat{a}_l\}, \quad (8)$$

where  $E_0$ ,  $f$ ,  $\Gamma$  and  $W$  represent normal-ordered zero-, one-, two- and three-body terms, respectively. In the IMSRG evolution, operators are truncated at the two-body level. By comparisons with other many-body methods, it had been estimated that the many-body uncertainty from the IMSRG evolution with the two-body normal-ordered approximation is about 2% in nuclear energy calculations [14, 15, 17, 27, 35, 90]. We have carefully calculated the ground-state energies of medium-mass nu-

TABLE I. Optimal  $c_D$  and  $c_E$  values, and calculated ground-state energies (in MeV) of  ${}^3\text{H}$  and  ${}^{16}\text{O}$ , compared with data [87]. The new local position-space Idaho potential [64] is used for the 2NF, while we construct a local or local-nonlocal (lnI) 3NF for this 2NF.

	$c_D$	$c_E$	$E({}^3\text{H})$	$E({}^{16}\text{O})$
3NF(local)	-2.0	-0.541	-8.78	-126.01
3NF(lnI)	6.0	0.894	-8.73	-127.15
Expt.			-8.482	-127.619

clei at closed shells by gradually increasing the  $c_D$  value with  $c_E$  also changing according to the relation obtained by the  $E({}^3\text{H})$  constraint. It is found that the calculated energies are monotonously lowered with increasing the  $c_D$  value. For the local 3NF regulator, calculations with  $c_D$  increasing starting from  $-6.0$  in a step of 1.0 show that  $c_D = -2.0$  gives good descriptions of experimental ground-state energies of the medium-mass closed-shell nuclei, as shown in the upper panel of Fig. 2. For the lnI 3NF regulator, calculations with  $c_D$  increasing starting from 2.0 in a step of 1.0 show that  $c_D = 6.0$  gives good descriptions of ground-state energies of the nuclei, see the lower panel of Fig. 2.

The optimal  $c_D$  and  $c_E$  values are summarized in Table I for the constructed 3NF with a local or lnI regulator. Note that we have only selected the integer values of  $c_D$  with a step of 1.0 in fitting, since errors (uncertainties) originating from IMSRG many-body and  $\chi\text{EFT}$  truncations are larger than the  $E({}^{16}\text{O})$  change caused by a change of one unit in the  $c_D$  value. This strategy is similar to that used in Ref. [35].

#### IV. APPLICATIONS TO THE CALCULATIONS OF NUCLEAR ENERGIES AND RADII

The constructed 3NF forms a family with the new local position-space 2NF proposed by the Idaho group [64]. We have used the new family of two- plus three-nucleon interactions to calculate the binding energies and charge radii of nuclei over a large range from  ${}^4\text{He}$  to  ${}^{132}\text{Sn}$ .

##### A. Closed-shell nuclei

For closed-shell nuclei, the single-reference IMSRG can be used to calculate energies and radii of the ground states. The model space is restricted by the single-particle basis truncation  $e = 2n + l \leq e_{\text{max}}$  and the 3NF matrix element truncation  $e_1 + e_2 + e_3 \leq E_{3\text{max}}$ . In this work, we use  $e_{\text{max}} = 14$  and  $E_{3\text{max}} = 24$  [96] with optimized HO frequencies ( $\hbar\Omega$ ) to ensure model-space convergence in all cases.

We compare the present calculations with those obtained using some other well-established interac-

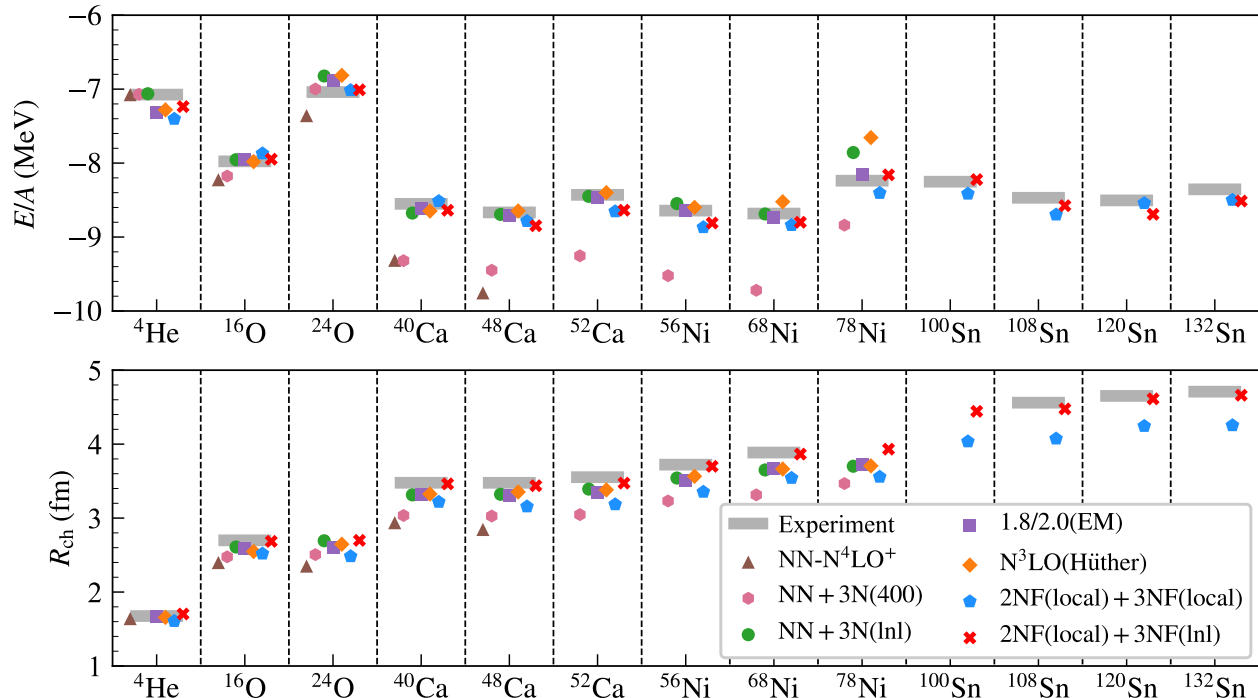


FIG. 3. Ground-state energies per nucleon and charge radii for selected doubly-closed-shell nuclei from  ${}^4\text{He}$  to  ${}^{132}\text{Sn}$ . The present calculations using our local and local-nonlocal 3NFs are labeled by  $2\text{NF}(\text{local})+3\text{NF}(\text{local})$  and  $2\text{NF}(\text{local})+3\text{NF}(\text{lnl})$ , respectively. They are compared with other 2NF-only calculations by the  $\text{NN}-\text{N}^4\text{LO}^+$  interaction [39], and 3NF-included calculations by  $\text{NN}+3\text{N}(400)$  [90, 92],  $\text{NN}+3\text{N}(\text{lnl})$  [32],  $1.8/2.0(\text{EM})$  [12, 30, 75] and  $\text{N}^3\text{LO}(\text{Hüther})$  [35]. Experimental data are taken from Refs. [87, 93–95].

tions, namely  $\text{NN}-\text{N}^4\text{LO}^+$  [39] (with  $\Lambda = 500$  MeV),  $\text{NN}+3\text{N}(400)$  [90, 92],  $\text{NN}+3\text{N}(\text{lnl})$  [32],  $1.8/2.0(\text{EM})$  [12, 30, 75] and  $\text{N}^3\text{LO}(\text{Hüther})$  (both 2NF and 3NF at  $\text{N}^3\text{LO}$  with  $\Lambda = 500$  MeV) [35], shown in Fig. 3. We see that the present  $2\text{NF}(\text{local})$  plus  $3\text{NF}(\text{local})$  family describes binding energies well, but underestimates charge radii in general. If we use the hybrid 3NF regulator of locality and nonlocality defined as Eq. (5), the family of  $2\text{NF}(\text{local})$  plus  $3\text{NF}(\text{lnl})$  gives the most accurate description of both binding energies and charge radii for the closed-shell nuclei from  ${}^4\text{He}$  to  ${}^{132}\text{Sn}$ , with deviations from experimental data below 2%, as shown in Fig. 3. The  $\text{lnl}$  3NF regulator scheme was suggested in Ref. [32], and tested with the family of a momentum-space  $\text{N}^3\text{LO}$  2NF [5] plus the  $\text{lnl}$   $\text{N}^2\text{LO}$  3NF [32]. While the  $\text{lnl}$  3NF regulator significantly improves the description of nuclear radii, calculated charge radii remain considerably smaller than experimental values [32]. Compared with this family based on the momentum-space 2NF plus the  $\text{lnl}$  3NF [labeled  $\text{NN}+3\text{N}(\text{lnl})$  in Fig. 3], the present family utilizes the new position-space 2NF plus the  $\text{lnl}$  3NF, but adopts a different fitting strategy to determine  $c_D$  and  $c_E$ . As shown in Fig. 3 with comparisons with other potentials, the present calculations with the new family of the local position-space  $\text{N}^3\text{LO}$  2NF plus the  $\text{lnl}$   $\text{N}^2\text{LO}$  3NF [labeled  $2\text{NF}(\text{local})+3\text{NF}(\text{lnl})$  in Fig. 3] gives the best de-

scription of both energies and radii, clearly better than calculations with the family of  $2\text{NF}(\text{local})+3\text{NF}(\text{local})$ .

## B. Open-shell nuclei

Open-shell nuclei can be calculated using the so-called valence-space IMSRG (VS-IMSRG) in which the valence-space effective Hamiltonian is obtained by the VS-IMSRG evolution [88]. Furthermore, to reduce the residual 3NF effect and choose a more appropriate shell-model core, the nucleus-dependent VS-IMSRG Hamiltonian with fractional filling of open-shell orbitals is used, named the ensemble normal ordering (ENO) [97]. The ENO VS-IMSRG evolution is also used to derive valence-space effective operators of other observables. The valence-space Hamiltonian is then diagonalized using the parallel shell model code `kshell1` [98]. In the present VS-IMSRG calculation, the valence space is defined as follows:  $p$  shell with  ${}^4\text{He}$  core for  ${}^{14}\text{O}$ ;  $sd$  shell with  ${}^{16}\text{O}$  core for  ${}^{17-28}\text{O}$ ,  ${}^{20-32}\text{Mg}$ ,  ${}^{22-34}\text{Si}$ ,  ${}^{28-36}\text{S}$ ,  ${}^{32-38}\text{Ar}$  and  ${}^{34-38}\text{Ca}$ ; proton  $sd$  and neutron  $pf$  shells with  ${}^{28}\text{O}$  core for  ${}^{34-40}\text{Mg}$ ,  ${}^{36-44}\text{Si}$ ,  ${}^{38-48}\text{S}$  and  ${}^{40-52}\text{Ar}$ ; and  $pf$  shell with  ${}^{40}\text{Ca}$  core for  ${}^{41-58}\text{Ca}$ .

Figure 4 shows the systematics of calculated ground-state energies, compared with experimental data, for oxy-

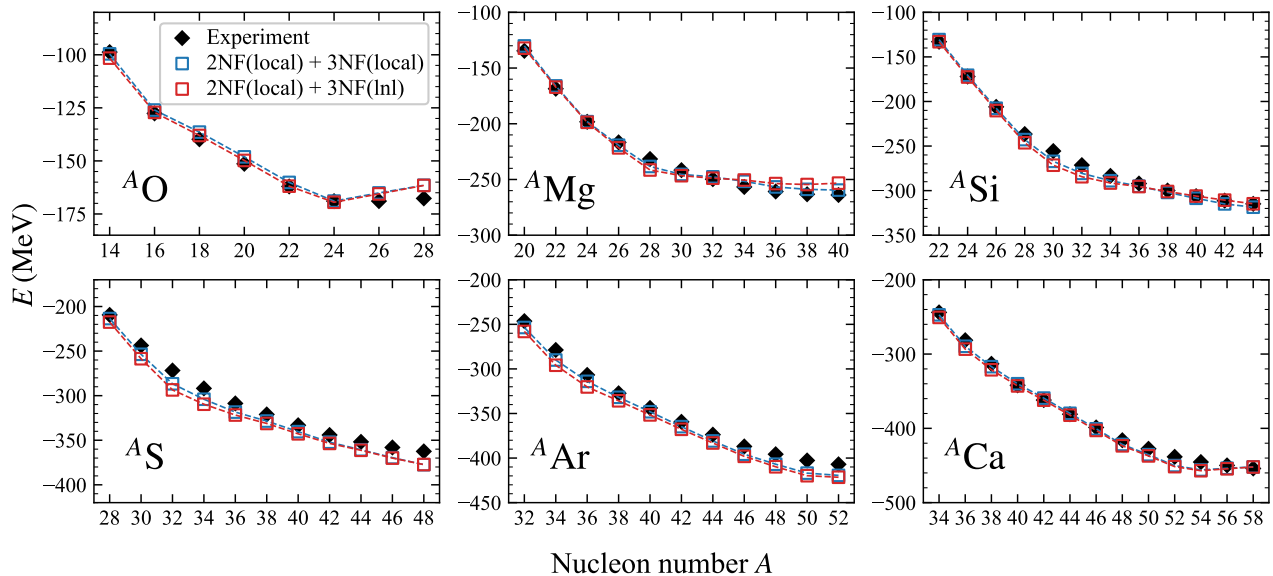


FIG. 4. Ground-state energies of O, Mg, Si, S, Ar and Ca isotopes, calculated in this work using the new families of the present 3NF (local or local-nonlocal) with the new Idaho position-space 2NF (local) within the many-body VS-IMSRG. Experimental data are taken from the 2020 atomic mass evaluation (AME2020) [87].

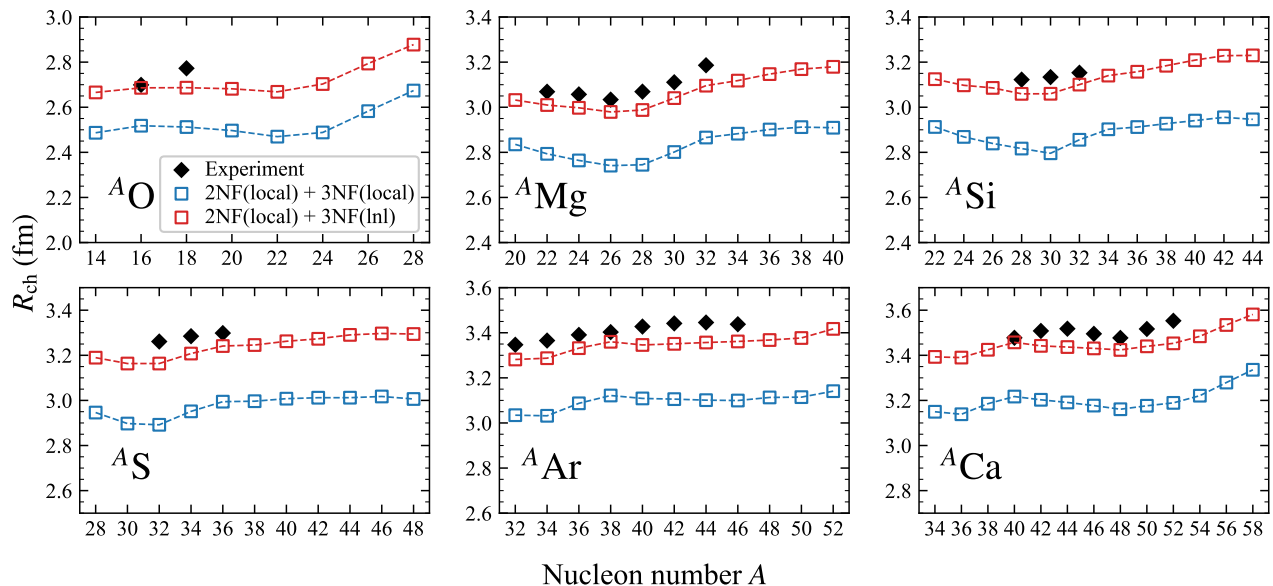


FIG. 5. Similar to Fig. 4 but for charge radii. Experimental charge radii are taken from Ref. [93–95].

gen, magnesium, silicon, sulfur, argon and calcium isotopic chains. We find that both local and lnl 3NFs give overall satisfying agreements with experimental ground-state energies for all isotopic chains investigated. Figure 5 shows charge radii for the isotopic chains studied. The situation is similar to closed-shell cases. The local-nonlocal  $N^2LO$  3NF connected to the new local position-space  $N^3LO$  2NF provides good description of charge radii, while local 3NF with the same position-space 2NF

underestimates the radii systematically. The change from a local 3NF regulator to a local-nonlocal 3NF regulator brings about 7% increase in the charge radius for medium-mass nuclei. The increase was also observed in previous studies [32, 99].

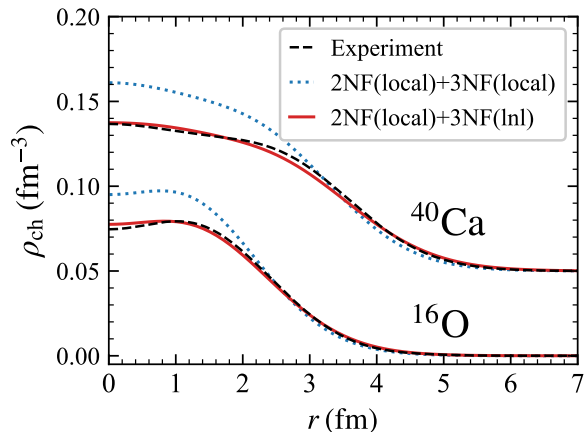


FIG. 6. Charge density distributions of  $^{16}\text{O}$  and  $^{40}\text{Ca}$ , calculated with 2NF(local)+3NF(local) and 2NF(local)+3NF(lnl), compared with experimental data [115]. The density of  $^{40}\text{Ca}$  is shifted by  $0.05 \text{ fm}^{-3}$  for better readability.

### C. Charge density distributions

Nuclear charge density distribution can provide more detailed information of nuclear structure, offering an even finer test for chiral Hamiltonians [32, 100, 101]. Such investigations have been carried out for decades also in *ab initio* calculations using a variety of many-body approaches and interactions [55, 99, 102–109]. Theoretically, the nuclear charge density can be calculated by folding the point-nucleon density with the intrinsic form factor of the free nucleons expressed in terms of the Sachs and Pauli form factors, see Refs. [99, 110, 111] for details of the calculation.

In this work, we focus on the charge densities of two representative closed-shell nuclei,  $^{16}\text{O}$  and  $^{40}\text{Ca}$ , whose experimental charge densities have been well measured. The converged calculations are performed using the single-reference IMSRG with  $e_{\text{max}} = 14$ ,  $E_{3\text{max}} = 24$  and an optimal HO frequency of  $\hbar\Omega = 16 \text{ MeV}$ . In both nuclei, charge density distributions calculated using 2NF(local)+3NF(lnl) are in excellent agreements with experimental data, while the densities obtained by 2NF(local)+3NF(local) are significantly larger than data in the central region of the nuclei, as shown in Fig. 6. The poorer description of the interior charge density obtained with the local 3NF may be attributed to the fact that local regulators are typically harder than their nonlocal counterparts, which may induce stronger short-range correlations [24]. The hybrid lnl regulator, by incorporating an additional nonlocal Gaussian factor, softens the short-range correlations, which results in a decrease in the interior density and an increase in the exterior density, thereby leading to an increased radius. Experimental measurements of nuclear charge density distribution re-

main a frontier area of nuclear physics studies [112–114]. Theoretical calculations of density distribution based on the first principles can provide deep insights into nucleon-nucleon interactions.

## V. SUMMARY

Understanding the properties of atomic nuclei from first principles represents a central challenge in nuclear physics. Within the framework of chiral effective field theory, nuclear forces are hierarchically organized, where three-nucleon forces emerge as a crucial component for accurate descriptions of nuclear structure. While significant progress has been made, it remains a persistent challenge to develop a unified chiral Hamiltonian that accurately describes both binding energies and charge radii across the nuclear chart.

In this work, we have constructed chiral three-nucleon forces at  $\text{N}^2\text{LO}$ , which form new families with the new high-quality local position-space two-nucleon interaction established by the Idaho group. The two low-energy constants,  $c_{\text{D}}$  and  $c_{\text{E}}$ , of the 3NF are constrained using the ground-state energies of  $^3\text{H}$  and  $^{16}\text{O}$ . We find that employing a local-nonlocal hybrid regularization scheme for the 3NF is particularly effective. The resulted chiral Hamiltonian is applied to nuclear many-body calculations, and provides the excellent description of both ground-state energies and charge radii for a wide range of nuclei from  $^4\text{He}$  up to  $^{132}\text{Sn}$ . This work highlights that the regularization scheme of the chiral 3NF can sensitively influence the quality of many-body predictions, especially for nuclear radii. The chiral Hamiltonian developed in this work should be useful for future high-precision *ab initio* calculations of nuclei.

## ACKNOWLEDGMENTS

The IMSRG calculations were performed using the `imsrg++` code [116], and chiral 3NF matrix elements were generated using the `NuHam1` code [96]. This work has been supported by the National Key R&D Program of China under Grants No. 2024YFA1610900, 2023YFA1606400; the National Natural Science Foundation of China under Grants No. 12335007, 12535008, 12441506. We acknowledge the High-Performance Computing Platform of Peking University for providing computational resources.

## DATA AVAILABILITY

The data that support the findings of this article are openly available [117].

- 
- [1] R. Machleidt, What is *ab initio*?, *Few-Body Syst.* **64**, 77 (2023).
- [2] A. Ekström, *et al.*, What is *ab initio* in nuclear theory?, *Front. Phys.* **11**, 1129094 (2023).
- [3] R. Machleidt and D. Entem, Chiral effective field theory and nuclear forces, *Phys. Rep.* **503**, 1 (2011).
- [4] H.-W. Hammer, S. König, and U. van Kolck, Nuclear effective field theory: Status and perspectives, *Rev. Mod. Phys.* **92**, 025004 (2020).
- [5] D. R. Entem and R. Machleidt, Accurate charge-dependent nucleon-nucleon potential at fourth order of chiral perturbation theory, *Phys. Rev. C* **68**, 041001 (2003).
- [6] E. Epelbaum, W. Glöckle, and U.-G. Meißner, The two-nucleon system at next-to-next-to-next-to-leading order, *Nucl. Phys. A* **747**, 362 (2005).
- [7] D. R. Entem, R. Machleidt, and Y. Nosyk, High-quality two-nucleon potentials up to fifth order of the chiral expansion, *Phys. Rev. C* **96**, 024004 (2017).
- [8] E. Epelbaum, H.-W. Hammer, and U.-G. Meißner, Modern theory of nuclear forces, *Rev. Mod. Phys.* **81**, 1773 (2009).
- [9] B. D. Carlsson, *et al.*, Uncertainty Analysis and Order-by-Order Optimization of Chiral Nuclear Interactions, *Phys. Rev. X* **6**, 011019 (2016).
- [10] H. Hergert, A Guided Tour of *ab initio* Nuclear Many-Body Theory, *Front. Phys.* **8**, 379 (2020).
- [11] R. Machleidt and F. Sammarruca, Recent advances in chiral EFT based nuclear forces and their applications, *Prog. Part. Nucl. Phys.* **137**, 104117 (2024).
- [12] S. R. Stroberg, J. D. Holt, A. Schwenk, and J. Simonis, *Ab Initio* Limits of Atomic Nuclei, *Phys. Rev. Lett.* **126**, 022501 (2021).
- [13] B. Hu *et al.*, *Ab initio* predictions link the neutron skin of  $^{208}\text{Pb}$  to nuclear forces, *Nat. Phys.* **18**, 1196 (2022).
- [14] B. C. He and S. R. Stroberg, Factorized approximation to the in-medium similarity renormalization group IM-SRG(3), *Phys. Rev. C* **110**, 044317 (2024).
- [15] S. R. Stroberg, T. D. Morris, and B. C. He, In-medium similarity renormalization group with flowing 3-body operators, and approximations thereof, *Phys. Rev. C* **110**, 044316 (2024).
- [16] A. Belley *et al.*, *Ab Initio* Uncertainty Quantification of Neutrinoless Double-Beta Decay in  $^{76}\text{Ge}$ , *Phys. Rev. Lett.* **132**, 182502 (2024).
- [17] H. Hergert, S. Binder, A. Calci, J. Langhammer, and R. Roth, *Ab Initio* Calculations of Even Oxygen Isotopes with Chiral Two-Plus-Three-Nucleon Interactions, *Phys. Rev. Lett.* **110**, 242501 (2013).
- [18] D. Lee, Recent Progress in Nuclear Lattice Simulations, *Front. Phys.* **8**, 174 (2020).
- [19] E. Epelbaum, H. Krebs, D. Lee, and U.-G. Meißner, *Ab Initio* Calculation of the Hoyle State, *Phys. Rev. Lett.* **106**, 192501 (2011).
- [20] S. Elhatisari, *et al.*, *Ab initio* alpha-alpha scattering, *Nature* **528**, 111–114 (2015).
- [21] S. Elhatisari, L. Bovermann, Y.-Z. Ma, and others., Wavefunction matching for solving quantum many-body problems, *Nature* **630**, 59–63 (2024).
- [22] S. Gandolfi, D. Lonardonì, A. Lovato, and M. Piarulli, Atomic Nuclei From Quantum Monte Carlo Calculations With Chiral EFT Interactions, *Front. Phys.* **8**, 117 (2020).
- [23] B. R. Barrett, P. Navrátil, and J. P. Vary, *Ab initio* no core shell model, *Prog. Part. Nucl. Phys.* **69**, 131–181 (2013).
- [24] K. Hebeler, Three-nucleon forces: Implementation and applications to atomic nuclei and dense matter, *Phys. Rep.* **890**, 1 (2021).
- [25] R. Machleidt and F. Sammarruca, Can chiral EFT give us satisfaction?, *Eur. Phys. J. A* **56**, 95 (2020).
- [26] F. Sammarruca and R. Millerson, Overview of symmetric nuclear matter properties from chiral interactions up to fourth order of the chiral expansion, *Phys. Rev. C* **104**, 064312 (2021).
- [27] S. Binder, J. Langhammer, A. Calci, and R. Roth, *Ab initio* path to heavy nuclei, *Phys. Lett. B* **736**, 119 (2014).
- [28] A. Ekström *et al.*, Optimized Chiral Nucleon-Nucleon Interaction at Next-to-Next-to-Leading Order, *Phys. Rev. Lett.* **110**, 192502 (2013).
- [29] J. Simonis, K. Hebeler, J. D. Holt, J. Menéndez, and A. Schwenk, Exploring *sd*-shell nuclei from two- and three-nucleon interactions with realistic saturation properties, *Phys. Rev. C* **93**, 011302 (2016).
- [30] J. Simonis, S. R. Stroberg, K. Hebeler, J. D. Holt, and A. Schwenk, Saturation with chiral interactions and consequences for finite nuclei, *Phys. Rev. C* **96**, 014303 (2017).
- [31] W. G. Jiang *et al.*, Accurate bulk properties of nuclei from  $A = 2$  to  $\infty$  from potentials with  $\Delta$  isobars, *Phys. Rev. C* **102**, 054301 (2020).
- [32] V. Somà, P. Navrátil, F. Raimondi, C. Barbieri, and T. Duguet, Novel chiral Hamiltonian and observables in light and medium-mass nuclei, *Phys. Rev. C* **101**, 014318 (2020).
- [33] F. Sammarruca, *et al.*, Toward order-by-order calculations of the nuclear and neutron matter equations of state in chiral effective field theory, *Phys. Rev. C* **91**, 054311 (2015).
- [34] F. Sammarruca, B. Chen, L. Coraggio, N. Itaco, and R. Machleidt, Dirac-Brueckner-Hartree-Fock versus chiral effective field theory, *Phys. Rev. C* **86**, 054317 (2012).
- [35] T. Hübner, K. Vobig, K. Hebeler, R. Machleidt, and R. Roth, Family of chiral two- plus three-nucleon interactions for accurate nuclear structure studies, *Phys. Lett. B* **808**, 135651 (2020).
- [36] C. Drischler, K. Hebeler, and A. Schwenk, Chiral Interactions up to Next-to-Next-to-Next-to-Leading Order and Nuclear Saturation, *Phys. Rev. Lett.* **122**, 042501 (2019).
- [37] E. Epelbaum *et al.* (LENPIC Collaboration), Few- and many-nucleon systems with semilocal coordinate-space regularized chiral two- and three-body forces, *Phys. Rev. C* **99**, 024313 (2019).
- [38] P. Maris *et al.* (LENPIC Collaboration), Light nuclei with semilocal momentum-space regularized chiral interactions up to third order, *Phys. Rev. C* **103**, 054001 (2021).
- [39] P. Maris *et al.* (LENPIC Collaboration), Nuclear properties with semilocal momentum-space regularized chi-

- ral interactions beyond  $N^2LO$ , *Phys. Rev. C* **106**, 064002 (2022).
- [40] F. Sammarruca and R. Millerson, Exploring the relationship between nuclear matter and finite nuclei with chiral two- and three-nucleon forces, *Phys. Rev. C* **102**, 034313 (2020).
- [41] M. C. Atkinson, W. H. Dickhoff, M. Piarulli, A. Rios, and R. B. Wiringa, Reexamining the relation between the binding energy of finite nuclei and the equation of state of infinite nuclear matter, *Phys. Rev. C* **102**, 044333 (2020).
- [42] W. G. Jiang, C. Forssén, T. Djärv, and G. Hagen, Nuclear-matter saturation and symmetry energy within  $\Delta$ -full chiral effective field theory, *Phys. Rev. C* **109**, L061302 (2024).
- [43] I. Svensson, A. Ekström, and C. Forssén, Inference of the low-energy constants in  $\Delta$ -full chiral effective field theory including a correlated truncation error, *Phys. Rev. C* **109**, 064003 (2024).
- [44] W. G. Jiang, C. Forssén, T. Djärv, and G. Hagen, Emulating *ab initio* computations of infinite nucleonic matter, *Phys. Rev. C* **109**, 064314 (2024).
- [45] F. Marino, W. G. Jiang, and S. J. Novario, Diagrammatic *ab initio* methods for infinite nuclear matter with modern chiral interactions, *Phys. Rev. C* **110**, 054322 (2024).
- [46] H. Krebs and E. Epelbaum, Toward consistent nuclear interactions from chiral Lagrangians. I. The path-integral approach, *Phys. Rev. C* **110**, 044003 (2024).
- [47] H. Krebs and E. Epelbaum, Toward consistent nuclear interactions from chiral Lagrangians. II. Symmetry preserving regularization, *Phys. Rev. C* **110**, 044004 (2024).
- [48] V. Springer, H. Krebs, and E. Epelbaum, Chiral  $3\pi$ -exchange potential using the method of unitary transformation, *Phys. Rev. C* **112**, 034004 (2025).
- [49] V. Cirigliano, M. Dawid, W. Dekens, and S. Reddy, New Class of Three-Nucleon Forces and Their Implications, *Phys. Rev. Lett.* **135**, 022501 (2025).
- [50] P. Arhuis, K. Hebeler, and A. Schwenk, Neutron-rich nuclei and neutron skins from chiral low-resolution interactions, *arXiv* (2024), 2401.06675.
- [51] B. S. Hu, *et al.*, The neutron dripline in calcium isotopes from a chiral interaction, *arXiv* (2025), 2512.11723.
- [52] R. Hu, *et al.*, *Ab initio* Exact Calculation of Strongly-Correlated Nucleonic Matter, *arXiv* (2026), 2508.09252.
- [53] J. Carlson *et al.*, Quantum Monte Carlo methods for nuclear physics, *Rev. Mod. Phys.* **87**, 1067 (2015).
- [54] D. Lonardonì, *et al.*, Properties of Nuclei up to  $A = 16$  using Local Chiral Interactions, *Phys. Rev. Lett.* **120**, 122502 (2018).
- [55] J. E. Lynn, *et al.*, Quantum Monte Carlo calculations of light nuclei with local chiral two- and three-nucleon interactions, *Phys. Rev. C* **96**, 054007 (2017).
- [56] R. Curry, R. Somasundaram, S. Gandolfi, A. Gezerlis, and I. Tews, Perturbative treatment of nonlocal chiral interactions in auxiliary-field diffusion Monte Carlo calculations, *Phys. Rev. C* **111**, 015801 (2025).
- [57] M. Piarulli, *et al.*, Local chiral potentials with  $\Delta$ -intermediate states and the structure of light nuclei, *Phys. Rev. C* **94**, 054007 (2016).
- [58] M. Piarulli, *et al.*, Light-Nuclei Spectra from Chiral Dynamics, *Phys. Rev. Lett.* **120**, 052503 (2018).
- [59] G. Chambers-Wall, *et al.*, Quantum Monte Carlo Calculations of Magnetic Form Factors in Light Nuclei, *Phys. Rev. Lett.* **133**, 212501 (2024).
- [60] G. B. King, *et al.*, Chiral effective field theory calculations of weak transitions in light nuclei, *Phys. Rev. C* **102**, 025501 (2020).
- [61] M. Piarulli, S. Pastore, R. B. Wiringa, S. Brusilow, and R. Lim, Densities and momentum distributions in  $A \leq 12$  nuclei from chiral effective field theory interactions, *Phys. Rev. C* **107**, 014314 (2023).
- [62] R. Somasundaram, J. E. Lynn, L. Huth, A. Schwenk, and I. Tews, Maximally local two-nucleon interactions at  $N^3LO$  in  $\Delta$ -less chiral effective field theory, *Phys. Rev. C* **109**, 034005 (2024).
- [63] G. Chambers-Wall, *et al.*, Magnetic structure of  $A \leq 10$  nuclei using the Norfolk nuclear models with quantum Monte Carlo methods, *Phys. Rev. C* **110**, 054316 (2024).
- [64] S. K. Saha, D. R. Entem, R. Machleidt, and Y. Nosyk, Local position-space two-nucleon potentials from leading to fourth order of chiral effective field theory, *Phys. Rev. C* **107**, 034002 (2023).
- [65] S. Bogner, R. Furnstahl, and A. Schwenk, From low-momentum interactions to nuclear structure, *Prog. Part. Nucl. Phys.* **65**, 94 (2010).
- [66] S. K. Bogner, R. J. Furnstahl, and R. J. Perry, Similarity renormalization group for nucleon-nucleon interactions, *Phys. Rev. C* **75**, 061001 (2007).
- [67] A. Kuşoğlu *et al.*, Direct Observation of Competing  $M1$  and  $M3$  Transitions in  $^{10}\text{B}$ , *Phys. Rev. Lett.* **133**, 072502 (2024).
- [68] P. Y. Wang, *et al.*, *Ab initio* calculations with a new local chiral  $N^3LO$  nucleon-nucleon force, *Phys. Rev. C* **109**, 064316 (2024).
- [69] U. van Kolck, Few-nucleon forces from chiral Lagrangians, *Phys. Rev. C* **49**, 2932 (1994).
- [70] E. Epelbaum *et al.*, Three-nucleon forces from chiral effective field theory, *Phys. Rev. C* **66**, 064001 (2002).
- [71] M. Hoferichter, J. Ruiz de Elvira, B. Kubis, and U.-G. Meißner, Matching Pion-Nucleon Roy-Steiner Equations to Chiral Perturbation Theory, *Phys. Rev. Lett.* **115**, 192301 (2015).
- [72] M. Hoferichter, J. Ruiz de Elvira, B. Kubis, and U.-G. Meißner, Roy-Steiner-equation analysis of pion-nucleon scattering, *Phys. Rep.* **625**, 1 (2016).
- [73] P. Navrátil, Local three-nucleon interaction from chiral effective field theory, *Few-Body Systems* **41**, 117–140 (2007).
- [74] P. Navrátil, V. G. Gueorguiev, J. P. Vary, W. E. Ormand, and A. Nogga, Structure of  $A = 10 - 13$  Nuclei with Two- Plus Three-Nucleon Interactions from Chiral Effective Field Theory, *Phys. Rev. Lett.* **99**, 042501 (2007).
- [75] K. Hebeler, S. K. Bogner, R. J. Furnstahl, A. Nogga, and A. Schwenk, Improved nuclear matter calculations from chiral low-momentum interactions, *Phys. Rev. C* **83**, 031301 (2011).
- [76] S. Wesolowski, *et al.*, Rigorous constraints on three-nucleon forces in chiral effective field theory from fast and accurate calculations of few-body observables, *Phys. Rev. C* **104**, 064001 (2021).
- [77] D. Gazit, S. Quaglioni, and P. Navrátil, Three-Nucleon Low-Energy Constants from the Consistency of Interactions and Currents in Chiral Effective Field Theory, *Phys. Rev. Lett.* **103**, 102502 (2009).

- [78] J. Menéndez, D. Gazit, and A. Schwenk, Chiral Two-Body Currents in Nuclei: Gamow-Teller Transitions and Neutrinoless Double-Beta Decay, *Phys. Rev. Lett.* **107**, 062501 (2011).
- [79] T.-S. Park, *et al.*, Parameter-free effective field theory calculation for the solar proton-fusion and hep processes, *Phys. Rev. C* **67**, 055206 (2003).
- [80] A. Ekström, *et al.*, Effects of Three-Nucleon Forces and Two-Body Currents on Gamow-Teller Strengths, *Phys. Rev. Lett.* **113**, 262504 (2014).
- [81] A. Gårdestig and D. R. Phillips, How Low-Energy Weak Reactions Can Constrain Three-Nucleon Forces and the Neutron-Neutron Scattering Length, *Phys. Rev. Lett.* **96**, 232301 (2006).
- [82] A. Baroni, R. Schiavilla, L. E. Marcucci, L. Girlanda, *et al.*, Local chiral interactions, the tritium Gamow-Teller matrix element, and the three-nucleon contact term, *Phys. Rev. C* **98**, 044003 (2018).
- [83] P. Navrátil, G. P. Kamuntavičius, and B. R. Barrett, Few-nucleon systems in a translationally invariant harmonic oscillator basis, *Phys. Rev. C* **61**, 044001 (2000).
- [84] E. Epelbaum, H. Krebs, and U.-G. Meißner, Improved chiral nucleon-nucleon potential up to next-to-next-to-next-to-leading order, *Eur. Phys. J. A* **51**, 53 (2015).
- [85] S. Binder *et al.* (LENPIC Collaboration), Few-nucleon systems with state-of-the-art chiral nucleon-nucleon forces, *Phys. Rev. C* **93**, 044002 (2016).
- [86] S. Binder *et al.* (LENPIC Collaboration), Few-nucleon and many-nucleon systems with semilocal coordinate-space regularized chiral nucleon-nucleon forces, *Phys. Rev. C* **98**, 014002 (2018).
- [87] M. Wang, W. Huang, F. Kondev, G. Audi, and S. Naimi, The AME 2020 atomic mass evaluation (II). Tables, graphs and references\*, *Chin. Phys. C* **45**, 030003 (2021).
- [88] K. Tsukiyama, S. K. Bogner, and A. Schwenk, In-Medium Similarity Renormalization Group For Nuclei, *Phys. Rev. Lett.* **106**, 222502 (2011).
- [89] T. D. Morris, N. M. Parzuchowski, and S. K. Bogner, Magnus expansion and in-medium similarity renormalization group, *Phys. Rev. C* **92**, 034331 (2015).
- [90] R. Roth, *et al.*, Medium-Mass Nuclei with Normal-Ordered Chiral  $NN+3N$  Interactions, *Phys. Rev. Lett.* **109**, 052501 (2012).
- [91] S. Zhang, *et al.*, The roles of three-nucleon force and continuum coupling in mirror symmetry breaking of oxygen mass region, *Phys. Lett. B* **827**, 136958 (2022).
- [92] V. Somà, A. Cipollone, C. Barbieri, P. Navrátil, and T. Duguet, Chiral two- and three-nucleon forces along medium-mass isotope chains, *Phys. Rev. C* **89**, 061301 (2014).
- [93] I. Angeli and K. Marinova, Table of experimental nuclear ground state charge radii: An update, *Atomic Data and Nuclear Data Tables* **99**, 69 (2013).
- [94] R. F. Garcia Ruiz and others., Unexpectedly large charge radii of neutron-rich calcium isotopes, *Nat. Phys.* **12**, 594–598 (2016).
- [95] F. Sommer and others., Charge Radii of  $^{55,56}\text{Ni}$  Reveal a Surprisingly Similar Behavior at  $N = 28$  in Ca and Ni Isotopes, *Phys. Rev. Lett.* **129**, 132501 (2022).
- [96] T. Miyagi, NuHamil : A numerical code to generate nuclear two- and three-body matrix elements from chiral effective field theory, *Eur. Phys. J. A* **59**, 150 (2023).
- [97] S. R. Stroberg, *et al.*, Nucleus-Dependent Valence-Space Approach to Nuclear Structure, *Phys. Rev. Lett.* **118**, 032502 (2017).
- [98] N. Shimizu, T. Mizusaki, Y. Utsuno, and Y. Tsunoda, Thick-restart block Lanczos method for large-scale shell-model calculations, *Comput. Phys. Commun.* **244**, 372 (2019).
- [99] V. Somà, C. Barbieri, T. Duguet, and P. Navrátil, Moving away from singly-magic nuclei with Gorkov Green's function theory, *Eur. Phys. J. A* **57**, 135 (2021).
- [100] B.-N. Lu, *et al.*, Essential elements for nuclear binding, *Phys. Lett. B* **797**, 134863 (2019).
- [101] A. Ekström *et al.*, Accurate nuclear radii and binding energies from a chiral interaction, *Phys. Rev. C* **91**, 051301 (2015).
- [102] T. Duguet, V. Somà, S. Lecluse, C. Barbieri, and P. Navrátil, *Ab initio* calculation of the potential bubble nucleus  $^{34}\text{Si}$ , *Phys. Rev. C* **95**, 034319 (2017).
- [103] S. Elhatisari, *et al.*, *Ab initio* Calculations of the Isotopic Dependence of Nuclear Clustering, *Phys. Rev. Lett.* **119**, 222505 (2017).
- [104] P. Arthuis, C. Barbieri, M. Vorabbi, and P. Finelli, *Ab Initio* Computation of Charge Densities for Sn and Xe Isotopes, *Phys. Rev. Lett.* **125**, 182501 (2020).
- [105] R. B. Wiringa, S. C. Pieper, J. Carlson, and V. R. Pandharipande, Quantum Monte Carlo calculations of  $A = 8$  nuclei, *Phys. Rev. C* **62**, 014001 (2000).
- [106] G. Hagen, A. Ekström, C. Forssén, G. R. Jansen, and others., Neutron and weak-charge distributions of the  $^{48}\text{Ca}$  nucleus, *Nat. Phys.* **12**, 186–190 (2015).
- [107] R. B. Wiringa, R. Schiavilla, S. C. Pieper, and J. Carlson, Neutron and nucleon-pair momentum distributions in  $A \leq 12$  nuclei, *Phys. Rev. C* **89**, 024305 (2014).
- [108] J. E. Lynn, *et al.*, Quantum Monte Carlo Calculations of Light Nuclei Using Chiral Potentials, *Phys. Rev. Lett.* **113**, 192501 (2014).
- [109] A. Gnech, A. Lovato, and N. Rocco, Static and dynamic properties of atomic nuclei with high-resolution potentials, *Phys. Rev. C* **111**, 024314 (2025).
- [110] J. W. Negele, Structure of Finite Nuclei in the Local-Density Approximation, *Phys. Rev. C* **1**, 1260 (1970).
- [111] P.-G. Reinhard and W. Nazarewicz, Nuclear charge densities in spherical and deformed nuclei: Toward precise calculations of charge radii, *Phys. Rev. C* **103**, 054310 (2021).
- [112] T. Suda *et al.*, Nuclear physics at the SCRIT electron scattering facility, *Prog. Theor. Exp. Phys.* **2012**, 03C008 (2012).
- [113] K. Tsukada *et al.*, First Elastic Electron Scattering from  $^{132}\text{Xe}$  at the SCRIT Facility, *Phys. Rev. Lett.* **118**, 262501 (2017).
- [114] A. Antonov *et al.*, The electron-ion scattering experiment ELISe at the International Facility for Antiproton and Ion Research (FAIR)—A conceptual design study, *Nucl. Instrum. Methods Phys. Res. Sect. A* **637**, 60 (2011).
- [115] H. De Vries, C. De Jager, and C. De Vries, Nuclear charge-density-distribution parameters from elastic electron scattering, *Atomic Data and Nuclear Data Tables* **36**, 495 (1987).
- [116] S. R. Stroberg, <https://github.com/ragnarstroberg/imsrg> (2024).
- [117] R. Hu *et al.*, Data: Chiral three-nucleon forces for the new local position-space two-nucleon potential in *ab ini-*

*tio* many-body calculations, [10.5281/zenodo.18516408](https://doi.org/10.5281/zenodo.18516408)  
(2026).